Transport and straining of *E. coli* O157:H7 in saturated porous media

Scott A. Bradford,[1] Jirka Simunek,[2] and Sharon L. Walker[3]

Received 13 December 2005; revised 9 May 2006; accepted 7 September 2006; published 18 November 2006.

[1] The transport and deposition behavior of pathogenic *Escherichia coli* O157:H7 was studied under unfavorable electrostatic conditions in saturated quartz sands of various sizes (710, 360, 240, and 150 μm) and at several flow rates. At a given velocity, column effluent breakthrough values for *E. coli* tended to decrease in magnitude, and concentration curves became more asymmetric with decreasing sand size. In a given sand, experiments conducted at a higher velocity tended to produce higher effluent concentrations, especially for finer (240 and 150 μm) textured sands. The shape of the deposition profiles for *E. coli* was also highly dependent on the sand size and velocity. Coarser-textured sands and higher flow rates were associated with less deposition and gradually decreasing concentrations with depth. Conversely, finer-textured sands and lower flow rates tended to produce greater deposition and nonmonotonic deposition profiles that exhibited a peak in retained concentration. This deposition peak occurred nearer to the column inlet for finer-textured sands and at low flow rates. Microscopic observations of *E. coli* retention in these finer-textured sands (micromodel experiments) clearly indicated that straining was the dominant mechanism of deposition. Batch experiments also indicated minor amounts of *E. coli* attachment for the selected sands and solution chemistry. A conceptual and numerical model was developed and successfully used to describe the observed *E. coli* transport and deposition data. Our conceptual model assumes that *E. coli* can aggregate when large numbers of monodispersed *E. coli* are deposited at pore constrictions or straining sites. When the deposited *E. coli* reach a critical concentration at the straining site, the aggregated *E. coli* O157:H7 can be released into aqueous solution as a result of hydrodynamic shearing forces.

Citation: Bradford, S. A., J. Simunek, and S. L. Walker (2006), Transport and straining of *E. coli* O157:H7 in saturated porous media, *Water Resour. Res.*, *42*, W12S12, doi:10.1029/2005WR004805.

1. Introduction

[2] *Escherichia coli* O157:H7 is a pathogenic bacteria strain that can inhabit the intestines of animals and humans. Gastrointestinal illness in infected individuals is characterized by severe cramping and bloody diarrhea due to the production of toxins that can damage the lining of the intestine. In a small percentage of cases, infection can lead to a life-threatening complication known as hemolytic uremic syndrome which involves the destruction of red blood cells and acute kidney failure (Centers for Disease Control and Prevention, *Escherichia coli* O157:H7, fact sheet, http://www.cdc.gov/ncidod/dbmd/diseaseinfo/escherichiacoli_g.htm). Surface and groundwater disease outbreaks have been associated with *E. coli* O157:H7 [*Geldreich et al.*, 1992; *U.S. Environmental Protection Agency* (*USEPA*), 2000; *O'Connor*, 2002] as well as other pathogenic bacteria. Water contamination by various strains of *E. coli* is becoming common in rural areas of the United States, with up to 40% of tested wells found to be contaminated [*USEPA*, 1997]. This is a problem of serious concern because of the low infectious dose for many pathogenic bacteria [*Loge et al.*, 2002]. Accurate knowledge of the processes that control the subsurface transport and survival of *E. coli* O157:H7 is therefore needed to assess contamination potential and to develop efficient water treatment techniques.

[3] Deposition of colloids in porous media has commonly been assumed to be controlled by attachment (collision with and fixation to the porous media), and therefore described using first-order attachment (clean bed filtration) theory [*Schijven and Hassanizadeh*, 2000; *Harvey and Harms*, 2002; *Jin and Flury*, 2002; *Ginn et al.*, 2002; *de Jonge et al.*, 2004]. In this case, an exponential decrease in retained concentration is predicted with transport distance. A growing body of literature, however, suggests that colloid deposition frequently does not agree with attachment theory predictions [*Camesano and Logan*, 1998; *Bolster et al.*, 1999; *Redman et al.*, 2001; *Bradford et al.*, 2002; *Tufenkji et al.*, 2003; *Li et al.*, 2004; *Tufenkji and Elimelech*, 2005a, 2005b; *Tong et al.*, 2005a, 2005b]. Deposition profiles for many types of colloids (latex microspheres, bacteria,

[1]George E. Brown Jr. Salinity Laboratory, ARS, USDA, Riverside, California, USA.
[2]Department of Environmental Sciences, University of California, Riverside, California, USA.
[3]Department of Chemical and Environmental Engineering, University of California, Riverside, California, USA.

0043-1397/06/2005WR004805$09.00

viruses, protists) have been reported to follow a hyperexponential (power law) profile distribution [*Albinger et al.*, 1994; *Baygents et al.*, 1998; *Simoni et al.*, 1998; *Bolster et al.*, 2000; *DeFlaun et al.*, 1997; *Zhang et al.*, 2001; *Redman et al.*, 2001; *Bradford et al.*, 2002; *Li et al.*, 2004; *Bradford and Bettahar*, 2005], implying a decreasing rate of deposition with increasing transport distance. Conversely, deposition profiles have also been reported to exhibit a peak at some distance down gradient from the source (nonmonotonic profile) [*Tong et al.*, 2005a].

[4] Various competing explanations have been proposed in the literature to explain nonexponential deposition profiles. These theories can be broadly classified as chemically or physically based. Chemical explanations that have been proposed include: porous media charge variability [*Johnson and Elimelech*, 1995], heterogeneity in surface charge characteristics of colloids [*Bolster et al.*, 1999; *Li et al.*, 2004], deposition of colloids in the secondary energy minimum of the Derjaguin-Landau-Verwey-Overbeek (DLVO) potential energy distribution [*Redman et al.*, 2004; *Hahn et al.*, 2004; *Tufenkji and Elimelech*, 2005b]; time-dependent deposition coefficients [*Tan et al.*, 1994; *Liu et al.*, 1995; *Camesano et al.*, 1999]; and colloid detachment [*Tufenkji et al.*, 2003]. Other researchers have proposed that nonexponential deposition profiles may occur as a result of physical factors that are not included in filtration theory, such as straining (deposition of colloids in smaller pores and at grain-grain junction) [*Bradford et al.*, 2002, 2003, 2004; *Li et al.*, 2004; *Tufenkji et al.*, 2004; *Bradford and Bettahar*, 2005; *Foppen et al.*, 2005], soil surface roughness [*Redman et al.*, 2001; *Kretzschmar et al.*, 1997], and hydrodynamic drag [*Li et al.*, 2005].

[5] Our ability to accurately predict the fate of pathogenic bacteria in the subsurface environment, such as *E. coli* O157:H7, is currently limited by our incomplete understanding of deposition mechanisms. The objective of this work is to systematically investigate the transport and deposition behavior of *E. coli* O157:H7 in several sized sands and at various flow rates. Results from batch, micromodel, and column experiments are used to deduce deposition mechanisms in these sands and the influence of system hydrodynamics on these processes. Data analysis and interpretation was aided through numerical modeling.

2. Materials and Methods

2.1. *E. coli* O157:H7

[6] *E. coli* O157:H7/pGFP strain 72 (Pina Fratamico, USDA-ARS-ERRC, Wyndmoor, PA) was used in the transport experiments. Green fluorescence in this bacteria is most strongly manifested when grown under oxygen rich conditions. To maximize fluorescence, *E. coli* O157:H7 was grown on tryptic soy agar plates (Becton, Dickinson and Co., Sparks, MD) with ampicillin (50 μg mL^{-1} final concentration). Plates were inoculated 3 days in a row to make sure that the final culture of bacteria was fully activated. After 15–18 hours of incubation, sterile water was placed on the plates and the colonies were gently harvested using a sterile glass rod to release the colonies into solution. The harvested colonies were then combined in a tube, and the bacteria were washed twice with phosphate-buffered saline (PBS) solution (FisherBiotech, Fair Lawn, NJ) by centrifugation at 2862 $\times$ g for 10 min and then resuspending in a 0.001 M NaBr solution. This 0.001 M NaBr solution consisted of deionized water buffered to pH 6.73 using 5×10^{-5} M $NaHCO_3$, and the solution electrical conductivity (EC) was 0.14 dS m^{-1}. This same 0.001 M NaBr solution was also used as eluant for the experiments.

[7] An approximate cell concentration of the bacterial stock was estimated using a calibration between optical density at 550 nm and measured cell concentration. The bacterial stock was then diluted to the desired concentrations in the NaBr solution for use in the column studies. The actual *E. coli* concentration in the influent solution was quantified using the spread plating method [*Clesceri et al.*, 1989] on tryptic soy agar plates with ampicillin (50 μg mL^{-1} final concentration). Plates were incubated at 37°C overnight and the concentrations were determined by enumeration. Colonies were confirmed under UV light.

[8] The relative concentrations of *E. coli* O157:H7 in liquid samples were determined using a Turner Quantech Fluorometer (Barnstead/Thermolyne, Dubuque, IA 52004-9910) equipped with excitation (490 nm: LE1095 $\times$ 13, NB490) and emission (515 nm: LE1095 $\times$ 23, SC515) filters. *E. coli* O157:H7 concentrations (average of triplicate measurements) were determined using calibration curves established between instrument response and standard solutions. The established calibration curves always had correlation coefficients very close to unity. This analytic protocol was sensitive to concentrations over two orders of magnitude below the initial concentration. Results from the fluorometer method discussed above were compared with the conventional spread plating technique in several *E. coli* O157:H7 transport experiments. Reasonable agreement between the two methods was obtained, although the fluorometer method provided a better mass balance. It should be noted that both spread plating and fluorometer techniques for quantifying *E. coli* concentrations are designed for monodispersed cell suspensions, if significant aggregation occurs then these methods may underestimate cell concentrations.

[9] The electrophoretic mobility and zeta potential of *E. coli* O157:H7 were measured in the 0.001 M NaBr solution to be -0.21 μm cm V^{-1} s^{-1}and -2.72 mV, respectively, using a ZetaPals instrument (Brookhaven Instruments Corporation, Holtsville, NY). The average size or effective diameter of *E. coli* O157:H7 was determined to be 1.16 μm using a Horiba LA 930 laser scattering particle size analyzer (Horiba Instruments, Irvine, CA 92614). This instrument was also used to verify the uniformity of the *E. coli* O157:H7 size distribution; i.e., normal distribution with a standard deviation of 0.31 μm. The hydrophobicity of *E. coli* O157:H7 was quantified by using the microbial adhesion to hydrocarbons (MATH) test [*Pembrey et al.*, 1999]. MATH test results indicated that approximately 64% of the cells partitioned into the hydrocarbon. Viability tests were performed using the Live/Dead BacLight kit (L-7012, Molecular Probles, Eugene, OR), and 100% of the cell were determined to be viable.

2.2. Sand

[10] Various sieve sizes of Ottawa aquifer sand (U.S. Silica, Ottawa, IL) were used in the soil column experi-

Table 1. Column Properties (Darcy Velocity, q; Porosity, ε; Column Length, L_c; and Pulse Duration, T_o) and the Effluent (M_{eff}), Sand (M_{sand}), and the Total (M_{total}) Mass Percentage Recovered for the Experimental Systems

d_{50}, μm	q, cm min^{-1}	ε	L_c, cm	T_o, min	M_{eff}	M_{sand}	M_{total}
710	0.031	0.334	12.53	150.0	78.2	23.7	101.9
710	0.114	0.357	12.97	75.0	82.4	3.2	85.6
710	0.196	0.330	12.45	37.5	80.1	8.5	88.6
360	0.024	0.341	12.66	150.0	54.3	43.2	97.5
360	0.099	0.333	12.50	75.0	73.0	5.8	78.8
360	0.196	0.348	12.80	37.5	68.1	10.4	78.5
240	0.026	0.324	12.35	150.0	9.2	85.0	94.2
240	0.097	0.332	12.49	75.0	42.1	30.4	72.5
150	0.017	0.334	10.00	150.0	0.3	95.9	96.2
150	0.102	0.341	12.66	75.0	13.2	52.4	65.6
150	0.177	0.350	10.00	37.5	47.0	33.8	80.8

ments. These sands were designated by their median grain size (d_{50}) as: 710, 360, 240, and 150 μm. The uniformity index ($U_i = d_{60}/d_{10}$ where x% of the mass was finer than d_x) of the 710, 360, 240, and 150 μm sands was measured to be 1.21, 1.88, 3.06, and 2.25, respectively. Pore size distribution information for these Ottawa sands can be calculated from capillary pressure–saturation curves presented by *Bradford and Abriola* [2001]. Ottawa sands typically consisted of 99.8% SiO_2 (quartz) and trace amounts of metal oxides, were spheroidal in shape, and had rough surfaces. Quartz sands possess a net negative charge at a neutral pH [*Redman et al.*, 2004].

2.3. Batch Experiments

[11] Batch experiments were conducted by placing 10 g of Ottawa sand (710, 360, 240, and 150 μm) and 10 mL of a known initial concentration of *E. coli* O157:H7 suspension into a 20 mL glass scintillation vial with the temperature kept at approximately 20°C. The suspension and sand were allowed to equilibrate for 4 hours at 150 rpm using an orbital shaker (Lab-Line, Melrose Park, IL). The initial and final concentrations of *E. coli* O157:H7 in the suspension were determining using the fluorometer and/or spread plate methods outlined above. A blank experiment (no sand) was also run to quantify the potential for *E. coli* O157:H7 growth or death in the 0.001 M NaBr solution at 20°C.

2.4. Column Experiments

[12] Column transport experiments were conducted to investigate the transport and deposition behavior of *E. coli* O157:H7 under unfavorable attachment conditions. Specifically, buffered solutions (neutral pH) with low ionic strength, quartz sands, and monodispersed cells were used. Borosilicate glass Kontes Chromaflex chromatography columns (Kimble/Kontes, Vineland, NJ) (15 cm long and 4.8 cm inside diameter) or stainless steel soil columns (10 cm long and 5.1 cm inside diameter) were used in the transport studies. The chromatography columns were equipped with a standard flangeless end fitting at the column bottom and a flow adapter at the top. The flow adapter allowed the column bed length to be adjusted, facilitating the tight sealing of the adapter at the soil surface. The manufacturer's bed support at the column inlet and outlet was replaced with a stainless steel wire screen (103 μm mesh spacing) supported by a coarser polyethylene screen to uniformly distribute the influent solution at the soil surface. The stainless steel columns were equipped with standard fittings and stainless steel wire screen at both of their ends. Tubing to and from the columns, fittings, column O-rings, and flow adapter were composed of chemically resistant materials such as Teflon, viton, stainless steel and Kalrez.

[13] *Bradford et al.* [2002] provided details on our methods for packing and cleaning the columns, and determining porosity. Table 1 provides porosity (ε) values and column lengths for each experimental soil column. A Masterflex L/S multihead drive pump (Barnant Company, Barrington, IL) equipped with standard heads was used to pump the *E. coli* O157:H7 suspension or eluant (0.001 M NaBr) solution upward through the vertically oriented columns at a steady rate. The average aqueous Darcy velocity (q) for the various column experiments is also given in Table 1, and the experimental temperature was approximately 20°C. Separate column experiments were conducted at different flow rates to better deduce the influence of hydrodynamics on *E. coli* O157:H7 deposition. The suspension was pumped upward to minimize any sedimentation that may occur as a result of the difference in density between the *E. coli* O157:H7 and eluant. The *E. coli* suspension was pumped through the columns for approximately 2 pore volumes (PV), after which a three-way valve was used to switch to the eluant for an additional 4 PV. Effluent samples were collected in glass test tubes over the course of each column experiment. *E. coli* O157:H7 concentrations in the effluent samples were determined using the fluorometer method discussed above. The maximum analytic error (twice the standard deviation) associated with triplicate relative concentration measurements was 0.028, and typically values were around 0.008.

[14] Following completion of the transport experiments, the deposition profile for *E. coli* O157:H7 retained in the sand was determined. The end fitting was removed and the saturated porous medium was carefully excavated into 50 mL Falcon tubes containing around 20 mL of 0.001 M NaBr solution. Approximately 8 tubes were recovered from a column, with each tube containing around 50 g of sand. The tubes were shaken for 15 min using an Eberbach shaker (Eberbach corporation, Ann Arbor, Michigan). The concentration of *E. coli* O157:H7 in the excess 0.001M NaBr solution was then measured using the previously discussed fluorometer method. The maximum analytic error (twice the standard deviation) associated with triplicate concentration measurements was 0.048, and typical values were around 0.01. Liquid and sand filled tubes were placed in an oven (200°C) overnight to volatilize the remaining solution from the sand. The volume of solution and mass of sand in each tube was determined from mass balance by measuring the weight of the empty tubes, liquid and sand filled tubes, and sand filled tubes.

[15] An *E. coli* O157:H7 number balance was conducted at the end of each soil column experiment using the effluent concentration data and the final deposition profiles. The calculated number of effluent and deposited *E. coli* O157:H7 was normalized by the total number of injected cells into a column. Table 1 presents the calculated effluent (M_{eff}), sand (M_{sand}) and the total ($M_{total} = M_{sand} + M_{eff}$) mass percentage recovered for the experimental systems.

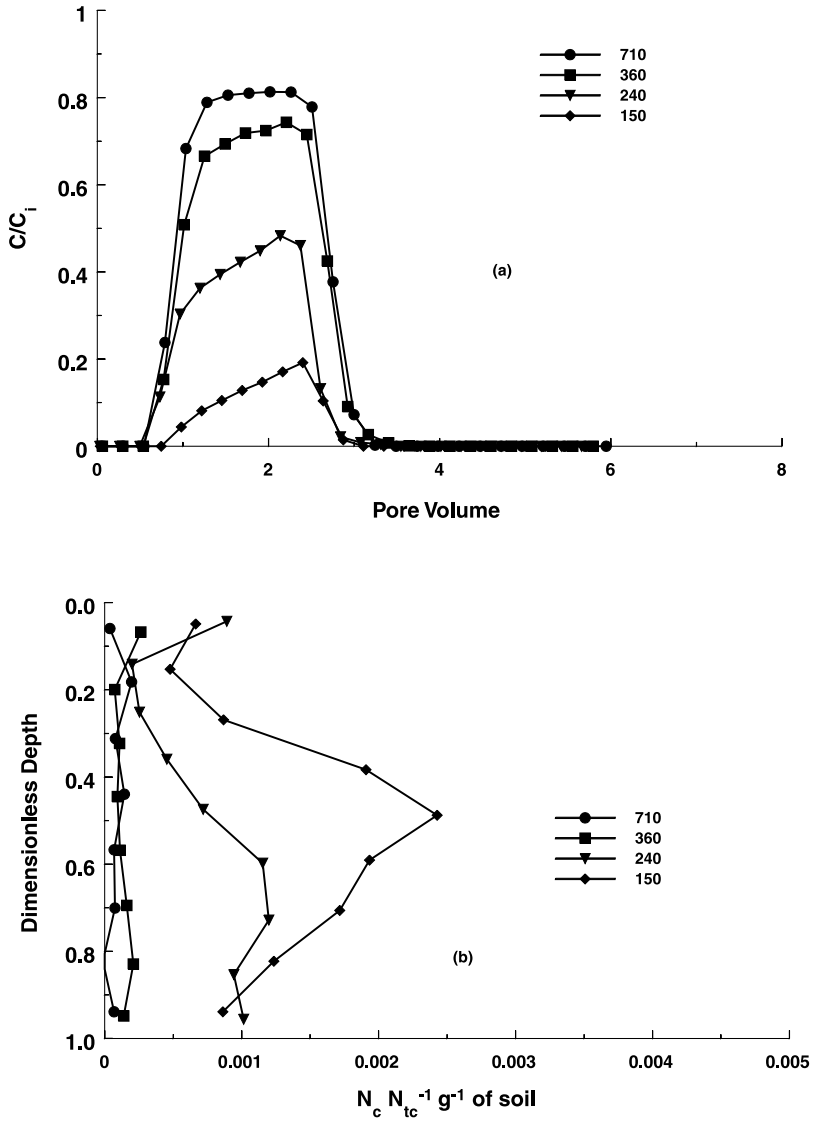

Figure 1. (a) Effluent concentration curves and (b) deposition profiles for *E. coli* O157:H7 in the 710, 360, 240, and 150 μm Ottawa sands at a Darcy velocity of around 0.1 cm min^{-1}. In Figure 1a, relative effluent concentrations (C/C_i) are plotted as a function of pore volumes, whereas in Figure 1b the normalized concentration (number of colloids, N_c, divided by the total number added to the column, N_{tc}) per gram of dry sand is plotted as a function of dimensionless distance (distance from the column inlet divided by the column length).

2.5. Micromodel Experiments

[16] Several transport experiments were conducted in a specially designed micromodel [*Bradford et al.*, 2005] to microscopically examine the deposition behavior of *E. coli* O157:H7 in 150 μm sand. The micromodel consists of a 0.2 cm thick by 2.0 cm wide by 7 cm long glass chamber (inside dimensions), with a glass tube (0.5 cm inside diameter) and septum assembly joined at both ends of the chamber. The tubing was connected to the chamber by a glass blower at an angle of about 45°, so that the micromodel could lay flat on a horizontal surface. During packing the micromodel chamber was oriented vertically without the top septum. The desired sands were then wet packed in the chamber. Hypodermic needles and Teflon tubing were used to connect the inlet side of the chamber to a LabAlliance chromatography pump (State College, PA 16803) and a reservoir on the outlet side of the chamber. To be consistent with the column experiments conducted at a Darcy velocity of around 0.1 cm min^{-1}, the *E. coli* O157:H7 suspension was pumped at a steady rate of 0.04 mL min^{-1} (Darcy velocity of 0.1 cm min^{-1}) for about 60 min (around 2.5 pore volumes), followed by 0.001 M NaBr solution for an additional 60 min. After completion of a transport experiment, the hypodermic needles were removed and the final deposition behavior of the fluorescent *E. coli* O157:H7 was microscopically examined at several locations distributed along the micromodel using a Leica DM IRB epifluorescent microscope (Leica Microsystems Inc., Bannockburn, IL 60015). Images were captured by connecting the microscope to a video monitor and computer system. Photographs (600 times magnification) were taken using various inten-

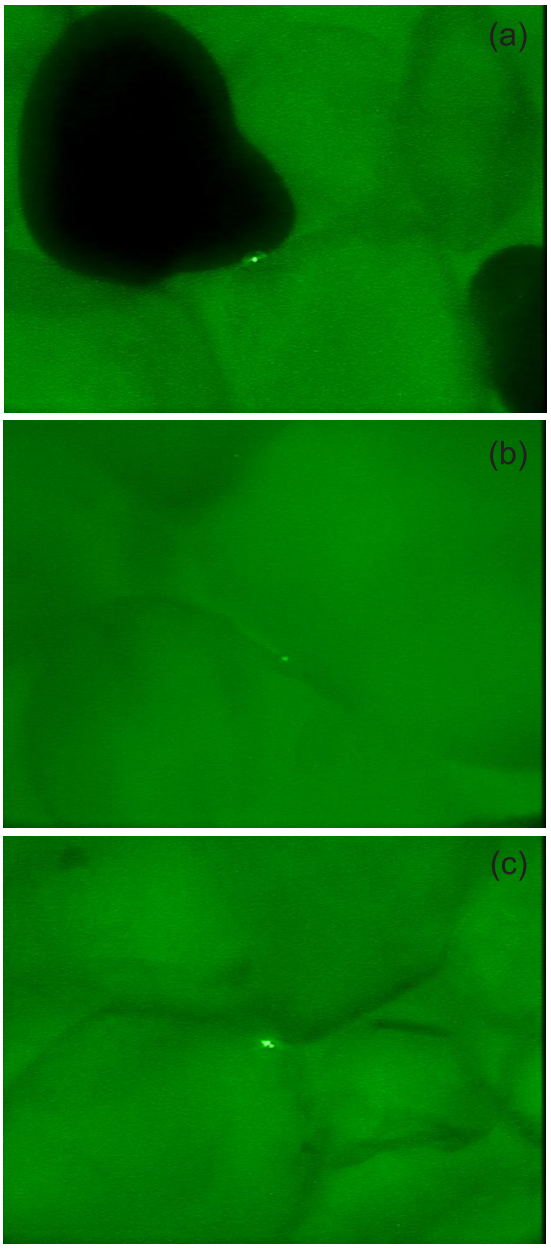

Figure 2. (a–c) Several representative micromodel photos (magnified 600 times) of *E. coli* O157:H7 deposition in the 150 μm sand. Photos were taken at several locations distributed along the micromodel. Grain surface roughness and differences in mineralogy (light and dark sand grains) are apparent in these photos. Fluorescent *E. coli* appear as bright particles in pore constrictions or on the solid surface.

sities of both UV and visible light so that sand grains and fluorescent bacteria could be visualized simultaneously.

3. Results and Discussion

3.1. Experiment

[17] Batch experiments were conducted to determine the maximum potential for *E. coli* O157:H7 attachment to the various Ottawa sands under the selected experimental conditions (20°C, pH = 6.73, low ionic strength = 0.001 M, negatively charged bacteria = −2.72 mV, and negatively charged quartz sand). A 4 hour equilibrium period was used in the batch experiments to be consistent with the column procedures, for which the average duration ranged from 2 to 7.5 hours depending on the water flow rate. Consistent with unfavorable attachment conditions, the initial and final concentrations of *E. coli* O157:H7 were almost identical (within a few percent of the initial concentration). This suggests that the presence of any metal oxides on the quartz sands had negligible influence on deposition. Similar results were obtained for the blank batch experiments conducted in the absence of sand, suggesting that the rates of bacteria growth and/or death were not significant during these experimental conditions.

[18] Column transport experiments were conducted to investigate the transport and deposition behavior of *E. coli* O157:H7 under unfavorable attachment conditions. Figure 1a presents effluent concentration curves for *E. coli* O157:H7 in the 710, 360, 240, and 150 μm sands at a Darcy velocity of around 0.1 cm min^{-1} (see Table 1 for values of q). Here relative effluent concentrations (C/C_i) are plotted as a function of pore volumes. The influent concentration was measured to be 1.7×10^8 CFU mL^{-1} using the spread plate method. Figure 1a demonstrates a systematic trend of decreasing peak effluent concentration with decreasing sand size. Table 1 indicates that M_{eff} ranged from 82 to 13% for the experiments conducted at approximately 0.1 cm min^{-1}. The effluent concentration curves for the finer-textured sands also exhibit asymmetric shapes, that slowly increased with continued addition of *E. coli* O157:H7 suspension. This implies a blocking or filling of favorable deposition sites.

[19] Figure 1b presents the deposition profiles for *E. coli* O157:H7 in the 710, 360, 240, and 150 μm sands at the end of these column experiments. Here the normalized concentration (number of colloids, N_c, divided by the total number added to the column, N_{tc}) per gram of dry sand is plotted as a function of dimensionless distance (distance from the column inlet divided by the column length). Consistent with the effluent curves, Table 1 indicates that the percent recovery of *E. coli* O157:H7 in the sands increased with decreasing sand size (3–52% for experiments conducted at around 0.1 cm min^{-1}). The total percent recovery for *E. coli* O157:H7 in the effluent and sands ranged from 86 to 66% (Table 1) at this velocity (0.1 cm min^{-1}). The shape of the deposition curve was highly dependent on the sand size. Deposition in the coarser-textured sands (710 and 360 μm) was rather uniform with increasing depth. In contrast, the finer-textured 240 and 150 μm sands exhibit an initial peak near the column inlet and a second larger peak at dimensionless depths of 0.73 and 0.49, respectively. The second deposition peak was also quite broad in the 240 and 150 μm sands, ranging in dimensionless depth from around 0.2 to 1.0.

[20] The mechanisms of *E. coli* O157:H7 deposition were further deduced by means of a micromodel experiment conducted in 150 μm sand at a Darcy velocity of 0.1 cm min^{-1}. Figure 2 presents several micromodel photos of *E. coli* O157:H7 deposition in the 150 μm sand. Additional photos of *E. coli* O157:H7 deposition in this 150 μm sand are presented by *Bradford et al.* [2006b]. All of these photos demonstrate that *E. coli* O157:H7 can be

Table 2. Fitted Values of Dispersivity (λ), Attachment Coefficient (k_{att}), and Detachment Coefficient (k_{det}) to the Effluent Concentration Curves of *E. coli* O157:H7 in the Various Sands When the Darcy Velocity is Around 0.1 cm min^{-1}[a]

d_{50}, μm	λ, cm	k_{att}, min^{-1}	k_{det}, min^{-1}	r^2_{eff}	MSE_{eff}	r^2_{sand}	MSE_{sand}
710	0.486	4.64E-3	0.32E-4	0.98	21.2E-4	0.18	2.86E-3
360	0.365	7.59E-3	0.01E-4	0.99	5.48E-4	0.00	5.18E-3
240	0.531	20.7E-3	0.01E-4	0.97	12.4E-4	0.41	15.5E-3
150	0.088	48.7E-3	1.97E-4	0.91	3.57E-4	0.24	64.5E-3

[a]Also included in this table is the coefficient of linear regression and mean square error for observed and simulated effluent (r_{eff}^2 and MSE_{eff}) and deposition (r_{sand}^2 and MSE_{sand}) data. Read 4.64E-3 as 4.64×10^{-3}.

deposited at grain junctions, small pores, and/or pore constrictions due to straining. The shape and surface roughness of the sand grains are also apparent in this photo. The light colored sand grains are predominately made from quartz, and the darker colored grains are believed to be associated with magnetite. Consistent with the batch experiments, a minimal amount of *E. coli* O157:H7 attachment was observed in the micromodel experiments.

[21] Attachment is not believed to be the dominant mechanism for *E. coli* O157:H7 deposition in the finer-textured media due to the following reasons. First, micromodel observations of *E. coli* O157:H7 retention in the 150 μm sand did not support the hypothesis that attachment was the controlling mechanism (see Figure 2). Second, the experimental conditions were designed to minimize the potential for *E. coli* O157:H7 attachment, specifically: the suspension was monodispersed, the porous medium was negatively charged, and the aqueous chemistry was selected to have a low ionic strength and buffered to a neutral pH. Third, the batch experiments suggest that a minimal amount of *E. coli* O157:H7 attachment occurred to the Ottawa sands. The experimental protocol for determining the deposition curves was also based upon the rapid release (15 min) of *E. coli* O157:H7 into solution under batch conditions and is not consistent with low desorption rates that are commonly observed in similar column experiments; i.e., the equilibrium concentration of colloids in solution is proportional to the desorption rate [e.g., *Schijven and Hassanizadeh*, 2000]. Finally, the *E. coli* O157:H7 deposition profiles in the 240 and 150 μm sands were not consistent with a first-order

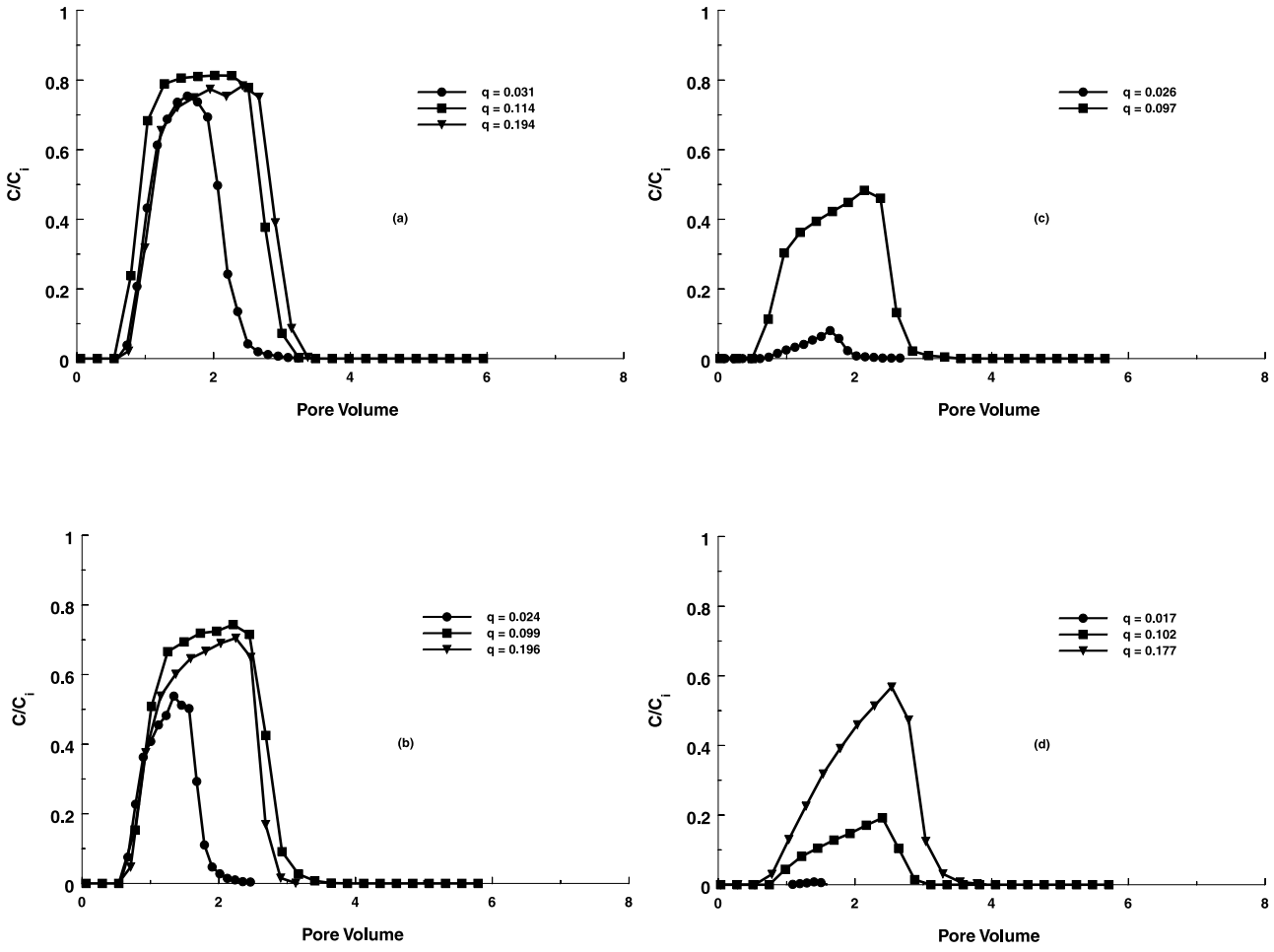

Figure 3. Effluent concentration curves for *E. coli* O157:H7 in the (a) 710, (b) 360, (c) 240, and (d) 150 μm Ottawa sands. The various experimental Darcy velocities are indicated in the figure legends and Table 1. The corresponding final deposition profiles are presented in Figures 4a–4d.

attachment-detachment model simulation (see following discussion and Table 2).

[22] Recent literature has attributed nonexponential deposition profiles to porous media charge variability [*Johnson and Elimelech*, 1995], heterogeneity in surface charge characteristics of colloids [*Bolster et al.*, 1999; *Li et al.*, 2004], and deposition of colloids in a secondary energy minimum [*Redman et al.*, 2004; *Tufenkji and Elimelech*, 2005b]. Other potential explanations for nonexponential deposition profiles include variability of the collector (grain) size and cell motility. We believe that these explanations are not consistent with our experimental data for the following reasons. First, solid surface charge heterogeneity and variability in the collector size is expected to be uniformly distributed throughout the sand depth, not at one particular location in the column. Second, the surface charge distribution characteristics for *E. coli* O157:H7 were the same for the various sand sizes. If surface charge distribution characteristics were controlling deposition, then a dependence on grain size would not be expected; i.e., only the deposition magnitude would increase, not the shape of the deposition curve. Third, deposition induced by attachment in the secondary minimum of the potential energy curve would not be expected to act preferentially in finer-textured sands or with depth. Fourth, no appreciable cell motility was observed in the Live/Dead cell analysis or in the micromodel experiments, and advective flow is expected to dominate over bacteria motility for the considered experimental conditions. Furthermore, cell motility is expected to be independent of the sand size.

[23] Micromodel observations shown in Figure 2 support our hypothesis that straining of *E. coli* O157:H7 is occurring in the 240 and 150 μm sands. Additional support for straining is based on the ratio of *E. coli* O157:H7 diameter (d_e) to the median grain diameter (d_{50}). The ratio of d_e/d_{50} was 0.005 and 0.007 for the 240 and 150 μm sands, respectively. *Bradford et al.* [2003] reported that straining of carboxyl latex microsphere occurred in these Ottawa sands when $d_e/d_{50} > 0.005$. Furthermore, *Bradford et al.* [2006a] found that particles larger than 1 μm were initially removed by 240 and 150 μm sands due to mechanical filtration and/or straining. Larger particles were transported in these sands with continued addition of suspension, presumably due to filling of straining sites. The asymmetric shape of the effluent concentration curves for *E. coli* O157:H7 in the 240 and 150 μm sands (Figure 1a) was consistent with this hypothesis.

[24] To further explore the role of system hydrodynamics on *E. coli* O157:H7 deposition additional experiments were conducted at several Darcy velocities in the various sands. Figures 3a–3d present effluent concentration curves for *E. coli* O157:H7 in the 710, 360, 240, and 150 μm sand, respectively. The various Darcy velocities are indicated in the figure legends and Table 1. Darcy velocity had a minimal influence on the breakthrough curves of the 710 and 360 μm sands. Conversely, increasing the Darcy velocity tended to produce a significant increase in the effluent concentration and M_{eff} (Table 1) in the finer-textured 240 and 150 μm sands.

[25] Figures 4a–4d present the corresponding deposition profiles for *E. coli* O157:H7 in the 710, 360, 240, and 150 μm sands, respectively. The shape of the deposition profile is highly dependent on the size of the sand and the Darcy velocity. Deposition profiles in the coarsest-textured 710 μm sand are similar in shape at different Darcy velocities. In contrast, deposition profiles in the finer-textured 360, 240, and 150 μm sands show a strong dependence on Darcy velocity. At higher Darcy velocities and in coarser-textured sands a more uniform distribution with depth is observed. The peak retained concentration is lower in magnitude and occurs further down gradient (at a greater depth) at higher Darcy velocities and for larger sand sizes. These observations suggest that straining of *E. coli* O157:H7 increases at lower velocities. This agrees with predicted straining behavior presented by *Cushing and Lawler* [1998]. Conversely, filtration theory predicts that the attachment coefficient will decrease with decreasing pore water velocity [e.g., *Logan et al.*, 1995]. We believe that hydrodynamic shear can diminish straining of *E. coli* O157:H7 at higher velocities and/or slowly mobilize strained bacteria down gradient (greater depth). *Tong et al.* [2005a] measured deposition curves for an adhesion deficit bacterial strain and observed deposition curves that were qualitatively similar to that shown in Figure 1b for the 150 μm sand. These authors found that slow mobilization of bacteria occurred mainly during bacteria injection. We therefore hypothesize that collisions between bacteria in suspension and those already removed from suspension and bound in a straining site, or in small pore space, may also play a role in bacteria removal and remobilization.

3.2. Theory and Model

[26] The HYDRUS-1D computer code [*Simunek et al.*, 2005] simulates water, heat, and multiple solute movement in one-dimensional variably saturated porous media, and is coupled to a nonlinear least squares optimization routine based upon the Marquardt-Levenberg algorithm [*Marquardt*, 1963] to facilitate the estimation of transport parameters from experimental data. HYDRUS-1D was modified as described below to simulate the transport and deposition of *E. coli* O157:H7 in the various sands. Our conceptual model assumes that *E. coli* can occur as monodispersed and aggregated species. Aggregation is hypothesized to occur when large numbers of monodispersed *E. coli* are deposited in straining sites as a result of flow induced collisions in small pore spaces (when hydrodynamic forces overcomes the electrostatic repulsion of deposited colloids). When the deposited *E. coli* reach a critical concentration in the straining site, the aggregated *E. coli* can be released into aqueous solution as a result of hydrodynamic shearing forces. The aggregated species can then be transported and deposited down gradient at a different rate than the monodispersed *E. coli*.

[27] In the absence of biological growth or death, a generalized form for the aqueous phase mass balance equation for monodispersed *E. coli* O157:H7 (species 1) is written as:

$$\frac{\partial(\theta_w C_1)}{\partial t} = -\nabla J_1 - \theta_w k_1 \Psi_1 C_1 + \rho_b k_{\det 1} S_1 \qquad (1)$$

where t is time [T; T denotes time units], ρ_b [M L^{-3}; M and L denote units of mass and length, respectively] is the soil bulk density, C_1 [N$_c$ L^{-3}; N$_c$ denotes number] is the liquid phase concentration of species 1, S_1 [N$_c$ M^{-1}] is the solid

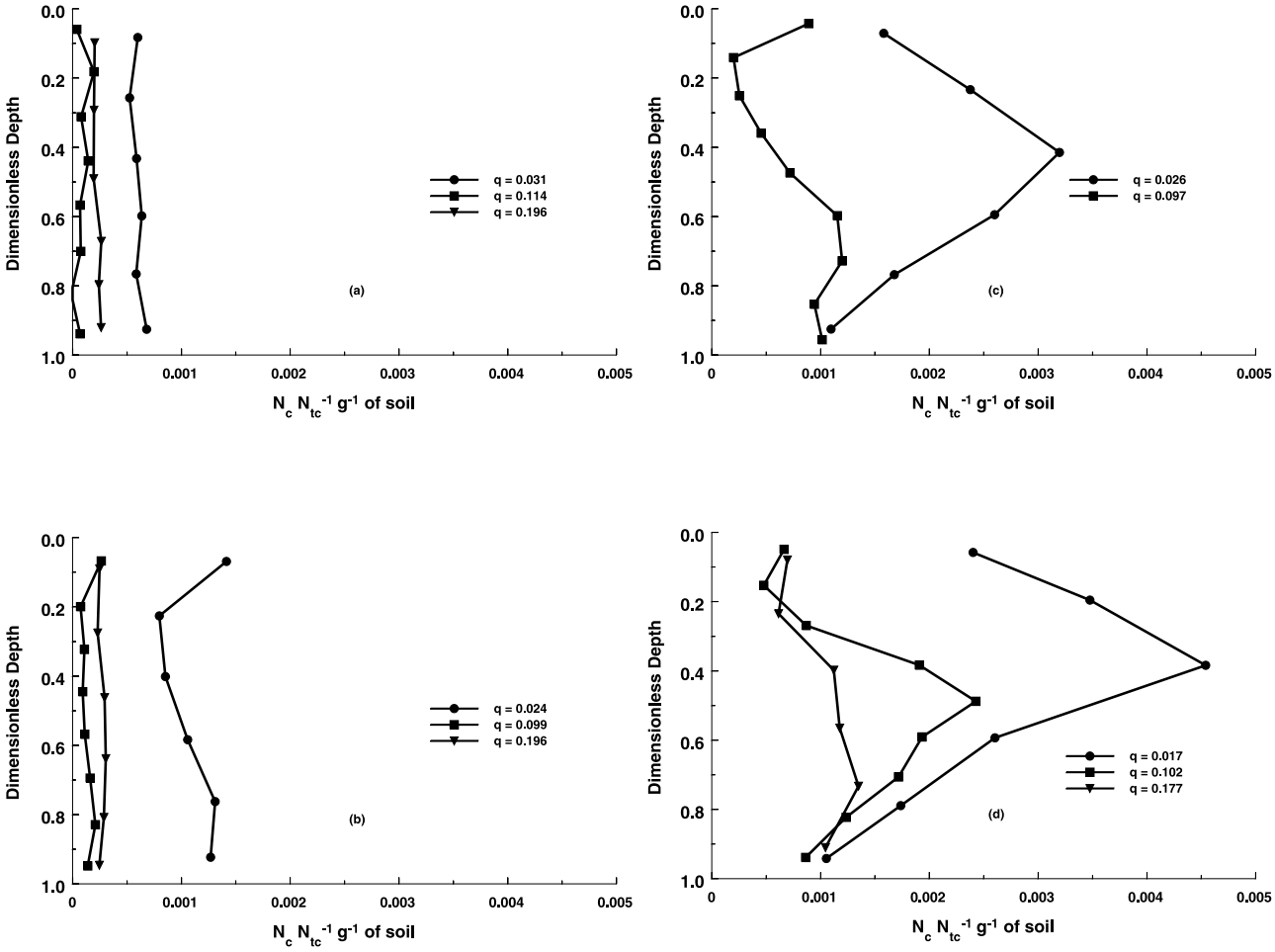

Figure 4. Final deposition profiles for *E. coli* O157:H7 in the (a) 710, (b) 360, (c) 240, and (d) 150 μm Ottawa sands. The various experimental Darcy velocities are indicated in the figure legends and Table 1. The corresponding effluent concentration curves are presented in Figures 3a–3d.

phase concentration of species 1, θ_w is the volumetric water content (dimensionless), k_1 [T^{-1}] is the first-order deposition coefficient, $k_{\mathrm{det}1}$ [T^{-1}] is the first-order detachment coefficient for species 1, J_1 [$N_c\ L^{-2}\ T^{-1}$] is the total solute flux for species 1, and ψ_1 (dimensionless) is a dimensionless deposition function for species 1. The first term on the right hand side of equation (1) accounts for advective, dispersive, and diffusive transport, whereas the second and third terms describe colloid deposition to and detachment from the solid phase.

[28] The solid phase mass balance equation for monodispersed *E. coli* O157:H7 (species 1) is given as:

$$\frac{\partial(\rho_b S_1)}{\partial t} = \theta_w k_1 \Psi_1 C_1 - \rho_b k_{\mathrm{det}\,1} S_1 - \rho_b k_{12} F_p \qquad (2)$$

Here k_{12} [T^{-1}] is the first-order production coefficient to account for the release rate of aggregated *E. coli* O157:H7 (species 2) into the aqueous phase, and F_p [$N_c\ M^{-1}$] is the aggregated species production function defined as the maximum of ($S_1 - S_{crit1}$) and 0; i.e., max($S_1 - S_{crit1}$, 0) where S_{crit1} [$N_c\ M^{-1}$] is the critical concentration of S_1 when production starts. For values of $S_1 < S_{crit1}$ no release of aggregated *E. coli* occurs and $F_p = 0$. As the small pore spaces begin to fill with *E. coli*, the deposition occurs at a greater distance from solid surface where the hydrodynamic shearing forces are greater. We hypothesis that a critical value of S_1 is reached, S_{crit1}, when *E. coli* can be released into the aqueous phase as an aggregated species ($F_p > 0$).

[29] If we assume that monodispersed *E. coli* is released as an aggregated species in the aqueous phase, then the mass balance equations for aggregated *E. coli* O157:H7 (species 2) in the aqueous and solid phases can be written in a manner analogous to equations (1) and (2) as

$$\frac{\partial(\theta_w C_2)}{\partial t} = -\nabla J_2 - \theta_w k_2 \Psi_2 C_2 + \rho_b k_{\mathrm{det}\,2} S_2 + \rho_b k_{12} F_p \qquad (3)$$

$$\frac{\partial(\rho_b S_2)}{\partial t} = \theta_w k_2 \Psi_2 C_2 - \rho_b k_{\mathrm{det}\,2} S_2 \qquad (4)$$

The subscripts 1 and 2 on parameters in these equations are used to distinguish monodispersed (species 1) and aggregated (species 2) *E. coli* O157:H7. Here liquid and solid phase concentrations of species 2 are written in terms of the number of monodispersed *E. coli*, so that consistent units are applied to both species 1 and 2, and to achieve an accurate mass balance.

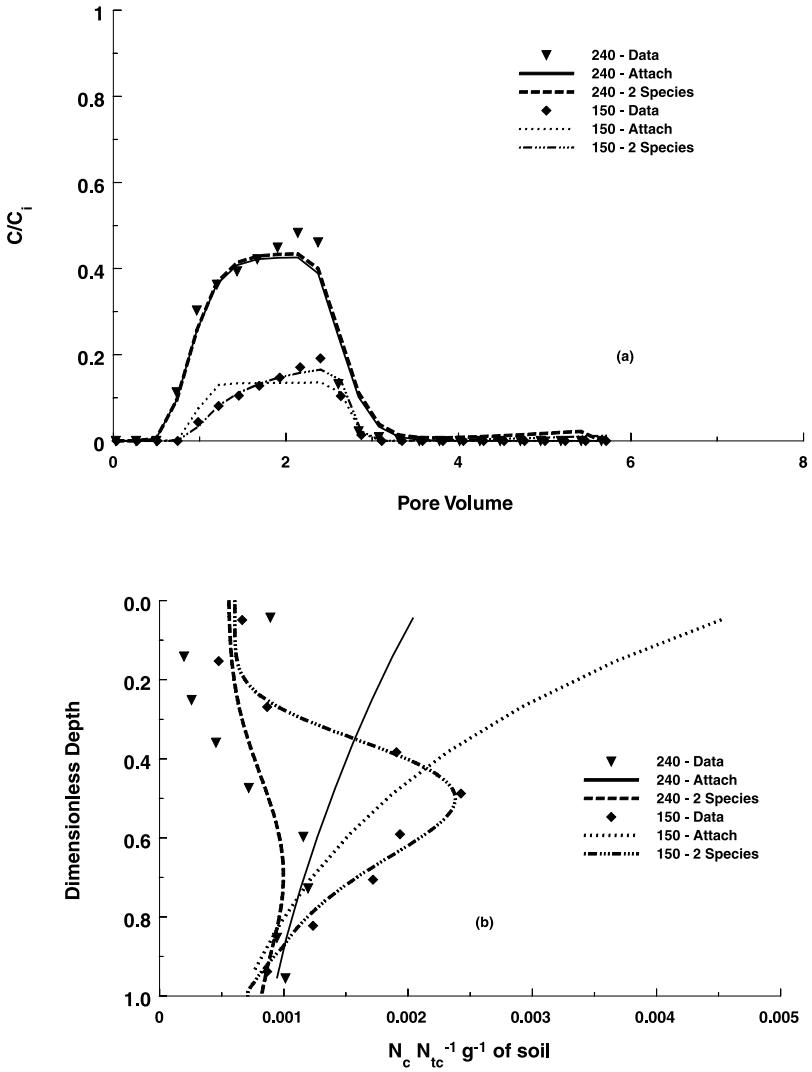

Figure 5. (a) Observed and simulated effluent concentration curves and (b) deposition profiles for *E. coli* O157:H7 in the 240 and 150 μm Ottawa sands at a Darcy velocity of around 0.1 cm min^{-1} (see Table 1 for values of q). The simulations in Figures 5a and 5b were based upon equations (1)–(5). The simulation labeled "Attach" considered only attachment and detachment by setting values of $k_{12} = 0$ and $\psi_1 = 1$, and model parameters are given in Table 2. The simulation labeled "2 Species" considered straining and both monodispersed and aggregated *E. coli* species, and model parameters are given in Table 3.

[30] An alternative model formation for the aggregated *E. Coli* (species 2) that is very similar to the above approach is to assume that the production term from species 1 to 2 (fourth term on the right hand side of equation (3)) occurs on the solid phase (equation (4)) instead of the liquid phase (equation (3)). This model was not pursued in this work for the following reasons. First, the existing model formulation provided an adequate description of the experimental data (see Figure 5 and the associated text below). Second, it was only possible to distinguish aggregated and monodispersed species of *E. coli* once they were released from solid phase; i.e., not when they were deposited in the pores. Finally, HYDRUS is a continuum model that determines average concentrations over a representative elementary pore volume, and therefore it can only simulate effective aggregation processes, not pore-scale details.

[31] To account for time and depth dependent deposition behavior a generalized form for ψ_1 is utilized as

$$\Psi_1 = \left(1 - \frac{S_1}{S_1^{\max}}\right)\left(\frac{d_{50} + z}{d_{50}}\right)^{-\beta_1} \tag{5}$$

where d_{50} [L] is the median grain size of the porous medium, β_1 (dimensionless) is a parameter that controls the shape of the spatial distribution of retained colloids for species 1 (i.e., the depth dependence of the deposition coefficient), $S_1^{\max}$ [N$_c$ M^{-1}] is the maximum solid phase concentration of deposited colloids for species 1, and z [L] is the down gradient distance from the porous medium inlet. A similar expression is used for ψ_2. The first term on the right hand side of equation (5) is used to account for blocking of favorable attachment sites or filling of straining sites (time dependent deposition)

Table 3. Fitted Model Parameters (λ, k_1, and S_1^{max} and, When Necessary, k_{12}, k_2, k_{det2}, and S_{crit1}) for *E. coli* O157:H7 Transport in the Various Sands[a]

d_{50}, μm	q, cm min^{-1}	λ, cm	k_1, min^{-1}	S_1^{max}, N$_c$ N$_{ic}^{-1}$ g^{-1}	k_{12}, min^{-1}	k_2, min^{-1}	k_{det2}, min^{-1}	S_{crit1}, N$_c$ N$_{ic}^{-1}$ g^{-1}	r^2
710[b]	0.031	0.214	0.002	1000.0	0.000	0.000	0.000	0.000	0.98
710[b]	0.114	0.486	0.004	1000.0	0.000	0.000	0.000	0.000	0.98
710[b]	0.196	0.160	0.012	1000.0	0.000	0.000	0.000	0.000	0.96
360[c]	0.024	0.703	0.023	1000.0	1.190	0.232	0.001	0.093	0.94
360[b]	0.099	0.365	0.007	1000.0	0.000	0.000	0.000	0.000	0.99
360[b]	0.196	0.199	0.021	0.306	0.000	0.000	0.000	0.000	0.99
240[c]	0.026	1.000	0.831	0.190	0.003	0.698	0.133	0.086	0.93
240[c]	0.097	0.531	0.175	1000.0	2.848	9.99	1.368	0.073	0.95
150[c]	0.017	0.088	0.255	1000.0	0.038	0.116	0.043	0.110	0.95
150[c]	0.102	0.088	0.853	0.179	2.254	2.195	0.211	0.084	0.98
150[c]	0.177	0.371	1.260	0.228	0.317	0.059	0.003	0.106	0.97

[a]Also included in this table is the coefficient of linear regression r^2. Values of $\beta_2 = 0.0$, $S_2^{max} = 1000.0$, and $k_{det1} = 0.0$ for all simulations.
[b]Simulations employed $\beta_1 = 0.0$.
[c]Simulations employed $\beta_1 = 0.432$.

according to the Langmuirian approach [*Deshpande and Shonnard*, 1999]. When the value of S_1^{max} is large then this term goes to 1, and time dependent deposition behavior is not considered. The second term on the right hand side of equation (5) is used to described depth dependent deposition behavior; i.e., decreasing deposition rates with depth. When β_1 goes to zero, then depth dependent deposition is not considered. Conversely, higher values of β_1 indicate an increasing depth dependence of the deposition coefficient, k_1. *Bradford et al.* [2003] found that the value of $\beta_1 = 0.432$ gave a good description of the spatial distribution of retained colloids when significant straining occurred in these same sands and for similar experimental conditions. In should be noted, however, that the optimal value of β_1 may also dependent the sand size, the solution chemistry, and hydrodynamics of a system. Straining has only recently been recognized as a potentially significant mechanism of colloid deposition, and additional research is needed to improve our understanding of this process under various hydrologic and solution chemistry conditions, and to relate straining model parameters to the collector efficiency of conventional filtration theory.

3.3. Simulations

[32] The model outlined above was solved numerically and used to simulate the transport and deposition of *E. coli* O157:H7 in the various sands. equations (1)–(5) reduce to the well known first-order attachment-detachment model when $k_{12} = 0$ and $\psi_1 = 1$. The *E. coli* O157:H7 transport data shown in Figures 1a and 1b were simulated using this first-order attachment-detachment model. Fitted values of the dispersivity (λ), the attachment coefficient (k_{att}) and detachment coefficient (k_{det}) are provided in Table 2, as well as the statistical parameters for the model fit to the data; i.e., the coefficient of linear regression and mean square error for effluent (r^2_{eff} and MSE_{eff}) and deposition (r^2_{sand} and MSE_{sand}) data. Table 2 indicates that the attachment-detachment model provided a good description of effluent data for *E. coli* O157:H7. Conversely, this model does not provide a satisfactory description of the *E. coli* O157:H7 deposition in these sands, especially in the finer-textured (240 and 150 μm) porous media (see r^2_{sand} and MSE_{sand} in Table 2).

[33] Figure 5a presents the observed and simulated effluent concentration curves for *E. coli* O157:H7 in the 240 and 150 μm sands at a Darcy velocity of around 0.1 cm min^{-1} (see Table 1 for values of q). Two simulations are shown for each data set. The first was the attachment/detachment model, and the second was the 2 species straining model that accounted for production of an aggregated species. The simulated curves for the 2 species model sums the contribution of monodispersed and aggregated *E. coli* concentrations together (both concentrations are written in terms of monodispersed *E. coli*). A summary of the fitted model parameters and statistical parameters characterizing the goodness of fit for the various model formulations is provided in Tables 2 and 3. Figure 5b presents the corresponding observed and simulated deposition profiles for these same systems. The effluent concentrations and the deposition profiles were reasonably described by the proposed 2 species straining model. Conversely, the attachment/detachment model does not accurately describe the experimental deposition profiles. The improved descriptive ability of the 2 species model can also be assessed by comparing statistical measures of the goodness of fit. The value of r^2_{sand} for the attachment/detachment and 2 species straining model was 0.41 and 0.59, respectively, for the 240 μm sand, and 0.24 and 0.98 for the 150 μm sands. We also calculated the Akaike information criterion (AIC) [*Akaike*, 1974] for these same data as a measure of goodness of fit that penalizes for adding fitting parameters; i.e., the model with the lowest value of AIC is preferred. The value of AIC for the attachment/detachment and 2 species straining model was 3.7 and -15.6, respectively, for the 240 μm sand, and 29.3 and 5.0 for the 150 μm sands. Hence values of AIC also indicate that the 2 species straining model provided a better description of the data than the attachment/detachment model.

[34] In the 240 and 150 μm sands, the 2 species model predicts breakthrough of a second peak for the aggregated *E. coli* (species 2) at later transport times and lower concentrations than for the monodispersed *E. coli* (species 1). Additional experimental studies and improved analytical sensitivity are necessary to fully verify this predicted behavior in our experimental systems. Bacteria transport data presented by *Tong et al.* [2005a], however, indicated that the peak concentration of nonmonotonic deposition profiles moved down gradient with increasing transport time (pore volumes). *Harter et al.* [2000] also observed a second peak (at later times) in the breakthrough curve for oocysts of *Cryptosporidium*.

[35] Although we cannot prove our hypothesis of *E. coli* aggregation, experimental evidence does support this line of reasoning. For example, micromodel observations of *E. coli* deposition shown in Figure 2 indicate that many cells can be retained in pore throats. *Crist et al.* [2005] also conducted DLVO calculations that examined the potential for colloid-colloid interactions. These calculations indicate that attractive hydrophobic forces may dominate the total potential interaction energies for colloids under conditions that otherwise (classical DLVO calculations) would produce repulsive conditions. Our MATH. tests for the *E. coli* O157:H7 indicate that 64% of the cells were hydrophobic, suggesting that favorable hydrophobic interactions were certainly possible for our experimental conditions.

[36] Table 3 provides a summary of the fitted model and statistical parameters for the 2 species model shown in Figure 5, as well as for the other experimental systems. Here the values of S_1^{max} of S_{crit1} were normalized by the initial number of bacteria in a unit volume of influent suspension, N_{ic}. Transport of *E. coli* in the 710 and 360 μm sands was adequately described using the first-order attachment and detachment model ($k_{12} = 0$, and $\psi_1 = 1$), with the one exception of the experiment in the 360 μm sand at the lowest velocity. In this case (low velocity and 360 μm sand), deviations between observed and simulated profiles suggest an additional retention mechanism, such as straining, may be involved in the cell deposition. An improved characterization of the transport behavior of *E. coli* in the 240 and 150 μm sands, however, required consideration of other processes. To simulate straining behavior of monodispersed *E. coli* O157:H7 we used $\beta_1 = 0.432$ and $k_{det1} = 0$, whereas $\psi_2 = 1$ for the second aggregated species was assumed. The values of k_1 and S_1^{max} control the shape of the breakthrough curve for monodispersed *E. coli* O157:H7, whereas values of k_{12}, S_{crit1}, k_2, and k_{det2} control the shape and evolution of the deposition profile and the second breakthrough curve. Systematic trends in model parameters were not obvious in Table 3, suggesting the potential for nonunique parameter estimates. Additional research is needed to fully assess and/or measure the range of applicability for these 2 species model parameters.

4. Summary and Conclusions

[37] The research presented herein indicates that straining can play a significant role in the transport and deposition behavior of *E. coli* O157:H7 in saturated sands under unfavorable attachment conditions. This finding was supported by micromodel observations of *E. coli* O157:H7 deposition at grain-grain junctions and in small pore spaces. Batch experiments also indicated that little *E. coli* O157:H7 attachment occurred between the quartz sand for the selected solution chemistry.

[38] In column experiments, straining tended to increase with decreasing sand size (increasingly smaller pores) and flow rate. Hydrodynamic shearing forces are believed to diminish colloid straining in these small pore spaces at higher flow rates. Most of the published research on colloid straining has been conducted using latex microspheres [*Bradford et al.*, 2002, 2003, 2004], or larger spherical protozoan parasites [*Bradford and Bettahar*, 2005; *Bradford et al.*, 2006a]. In these cases, deposition profiles followed an inverse power law (hyperexponential) distribution with increasing depth. The experimental results of this study indicate that nonmonotonic deposition profiles can also occur as a result of straining. Differences in the shape of the nonmonotonic deposition profiles were demonstrated to be a function of the sand size and the system hydrodynamics.

[39] A conceptual and mathematical modeling framework was proposed to account for the observed *E. coli* O157:H7 transport and deposition. This model assumes that *E. coli* O157:H7 aggregation occurs when large numbers of monodispersed *E. coli* O157:H7 are deposited in straining sites as a result of flow induced collisions in small pore spaces (when hydrodynamic forces overcome the electrostatic repulsion of deposited colloids). When the deposited *E. coli* O157:H7 reaches a critical concentration in the straining site, the aggregated cells can be released into aqueous solution as a result of hydrodynamic shearing forces. The aggregated species can then be transported and deposited down gradient at a different rate than the monodispersed *E. coli* O157:H7. This conceptual model was numerically implemented into the HYDRUS computer code and successfully used to describe the experimental data.

[40] Experimental evidence discussed above indicates that straining is likely to be an important mechanism of *E. coli* O157:H7 deposition in the finer-textured sands under unfavorable attachment conditions. Results also suggest that colloid-colloid interactions and system hydrodynamic influence straining processes. Additional research is warranted to better quantify and model the influence of these factors on straining deposition and mobilization, as well as the potential influence of colloid chemistry and shape, cell membrane rigidity and motility, and solution chemistry. This information is believed to be essential for predicting the fate of colloids and colloid associated contaminants in natural subsurface environments.

[41] **Acknowledgments.** This research was supported by the 206 Manure and Byproduct Utilization Project of the USDA-ARS. Mention of trade names and company names in this manuscript does not imply any endorsement or preferential treatment by the USDA. We would also like to acknowledge the valuable assistance of Yadata F. Tadassa in the experimental aspects of this research.

References

Akaike, H. (1974), A new look at statistical model identification, *IEEE Trans. Autom. Control*, *19*, 716–722.

Albinger, O., B. K. Biesemeyer, R. G. Arnold, and B. E. Logan (1994), Effect of bacterial heterogeneity on adhesion to uniform collectors by monoclonal populations, *FEMS Microbiol. Lett.*, *124*(3), 321–326.

Baygents, J. C., J. R. Glynn Jr., O. Albinger, B. K. Biesemeyer, K. L. Ogden, and R. G. Arnold (1998), Variation of surface charge density in monoclonal bacterial populations: Implications for transport through porous media, *Environ. Sci. Technol.*, *32*, 1596–1603.

Bolster, C. H., A. L. Mills, G. M. Hornberger, and J. S. Herman (1999), Spatial distribution of deposited bacteria following miscible displacement experiments in intact cores, *Water Resour. Res.*, *35*, 1797–1807.

Bolster, C. H., A. L. Mills, G. Hornberger, and J. Herman (2000), Effect of intra-population variability on the long-distance transport of bacteria, *Ground Water*, *38*(3), 370–375.

Bradford, S. A., and L. M. Abriola (2001), Dissolution of residual tetrachloroethylene in fractional wettability porous media: Incorporation of interfacial area estimates, *Water Resour. Res.*, *37*, 1183–1195.

Bradford, S. A., and M. Bettahar (2005), Straining, attachment, and detachment, of *Cryptosporidium* oocysts in saturated porous media, *J. Environ. Qual.*, *34*, 469–478.

Bradford, S. A., S. R. Yates, M. Bettahar, and J. Simunek (2002), Physical factors affecting the transport and fate of colloids in saturated porous media, *Water Resour. Res.*, *38*(12), 1327, doi:10.1029/2002WR001340.

Bradford, S. A., J. Simunek, M. Bettahar, M. T. van Genuchten, and S. R. Yates (2003), Modeling colloid attachment, straining, and exclusion in saturated porous media, *Environ. Sci. Technol.*, *37*, 2242–2250.

Bradford, S. A., M. Bettahar, J. Simunek, and M. T. van Genuchten (2004), Straining and attachment of colloids in physically heterogeneous porous media, *Vadose Zone J.*, *3*, 384–394.

Bradford, S. A., J. Simunek, M. Bettahar, Y. F. Tadassa, M. T. van Genuchten, and S. R. Yates (2005), Straining of colloids at textural interfaces, *Water Resour. Res.*, *41*, W10404, doi:10.1029/2004WR003675.

Bradford, S. A., Y. F. Tadassa, and Y. A. Pachepsky (2006a), Transport of *Giardia* and manure suspensions in saturated porous media, *J. Environ. Qual.*, *35*, 749–757.

Bradford, S. A., J. Simunek, M. Bettahar, M. T. van Genuchten, and S. R. Yates (2006b), Significance of straining in colloid deposition: Evidence and implications, *Water Resour. Res.*, *42*, W12S15, doi:10.1029/2005WR004791.

Camesano, T. A., and B. E. Logan (1998), Influence of fluid velocity and cell concentration on the transport of motile and nonmotile bacteria in porous media, *Environ. Sci. Technol.*, *32*, 1699–1708.

Camesano, T. A., K. M. Unice, and B. E. Logan (1999), Blocking and ripening of colloids in porous media and their implications for bacterial transport, *Colloids Surf. A*, *160*(3), 291–308.

Clesceri, L. S., A. E. Greenberg, and R. R. Trussell (1989), *Standard Methods for the Examination of Water and Wastewater*, 17th ed., Am. Public Health Assoc., Washington, D. C.

Crist, J. T., Y. Zevi, J. F. McCarthy, J. A. Throop, and T. S. Steenuis (2005), Transport and retention mechanisms of colloids in partially saturated porous media, *Vadose Zone J.*, *4*, 184–195.

Cushing, R. S., and D. F. Lawler (1998), Depth filtration: Fundamental investigation through three-dimensional trajectory analysis, *Environ. Sci. Technol.*, *32*, 3793–3801.

DeFlaun, M. F., C. J. Murray, M. Holben, T. Scheibe, A. Mills, T. Ginn, T. Griffin, E. Majer, and J. L. Wilson (1997), Preliminary observations on bacterial transport in a coastal plain aquifer, *FEMS Microbiol. Rev.*, *20*(3–4), 473–487.

de Jonge, L. W., C. Kjaergaard, and P. Moldrup (2004), Colloids and colloid-facilitated transport of contaminants in soils: An introduction, *Vadose Zone J.*, *3*, 321–325.

Deshpande, P. A., and D. R. Shonnard (1999), Modeling the effects of systematic variation in ionic strength on the attachment kinetics of *Pseudomonas fluorescens* UPER-1 in saturated sand columns, *Water Resour. Res.*, *35*, 1619–1627.

Foppen, J. W. A., A. Mporokoso, and J. F. Schijven (2005), Determining straining of *Escherichia coli* from breakthrough curves, *J. Contam. Hydrol.*, *76*, 191–210.

Geldreich, E. E., K. R. Fox, J. A. Goodrich, E. W. Rice, R. M. Clark, and D. L. Swerdlow (1992), Searching for a water supply connection in the Cabool, Missouri disease outbreak of *Escherichia Coli* O157:H7, *Water Res.*, *26*(8), 1127–1137.

Ginn, T. R., B. D. Wood, K. E. Nelson, T. D. Schiebe, E. M. Murphy, and T. P. Clement (2002), Processes in microbial transport in the natural subsurface, *Adv. Water Resour.*, *25*, 1017–1042.

Hahn, M. W., D. Abadzic, and C. R. O'Melia (2004), Aquasols: On the role of secondary minima, *Environ. Sci. Technol.*, *38*, 5915–5924.

Harter, T., S. Wagner, and E. R. Atwill (2000), Colloid transport and filtration of *Cryptosporidium parvum* in sandy soils and aquifer sediments, *Environ. Sci. Technol.*, *34*, 62–70.

Harvey, R. W., and H. Harms (2002), Transport of microorganisms in the terrestrial subsurface: In situ and laboratory methods, in *Manual of Environmental Microbiology*, 2nd ed., edited by C. J. Hurst et al., pp. 753–776, ASM Press, Washington, D. C.

Jin, Y., and M. Flury (2002), Fate and transport of viruses in porous media, *Adv. Agron.*, *77*, 39–102.

Johnson, P. R., and M. Elimelech (1995), Dynamics of colloid deposition in porous media: Blocking based on random sequential adsorption, *Langmuir*, *11*, 801–812.

Kretzschmar, R., K. Barmettler, D. Grolimun, Y. D. Yan, M. Borkovec, and H. Sticher (1997), Experimental determination of colloid deposition rates and collision efficiencies in natural porous media, *Water Resour. Res.*, *33*, 1129–1137.

Li, X., T. D. Scheibe, and W. P. Johnson (2004), Apparent decreases in colloid deposition rate coefficient with distance of transport under unfavorable deposition conditions: A general phenomenon, *Environ. Sci. Technol.*, *38*, 5616–5625.

Li, X., P. Zhang, C. L. Lin, and W. P. Johnson (2005), Role of hydrodynamic drag on microsphere deposition and re-entrainment in porous media under unfavorable conditions, *Environ. Sci. Technol.*, *39*, 4012–4020.

Liu, D., P. R. Johnson, and M. Elimelech (1995), Colloid deposition dynamics in flow-through porous media: Role of electrolyte concentration, *Environ. Sci. Technol.*, *29*, 2963–2973.

Logan, B. E., D. G. Jewett, R. G. Arnold, E. J. Bouwer, and C. R. O'Melia (1995), Clarification of clean-bed filtration models, *J. Environ. Eng.*, *121*, 869–873.

Loge, F. J., D. E. Thompson, and R. C. Douglas (2002), PCR detection of specific pathogens in water: A risk-based analysis, *Environ. Sci. Technol.*, *36*, 2754–2759.

Marquardt, D. W. (1963), An algorithm for least-squares estimation of nonlinear parameters, *J. Soc. Ind. Appl. Math.*, *11*, 431–441.

O'Connor, D. (2002), A summary report of the Walkerton inquiry: The events of May 2000 and related issues, Queen's Printer for Ontario, Toronto, Ontario, Canada.

Pembrey, R. S., K. C. Marshall, and R. P. Schneider (1999), Cell surface analysis techniques: What do cell preparation protocols do to cell surface properties?, *Appl. Environ. Microbiol.*, *65*, 2877–2894.

Redman, J. A., S. B. Grant, T. M. Olson, and M. K. Estes (2001), Pathogen filtration, heterogeneity, and the potable reuse of wastewater, *Environ. Sci. Technol.*, *35*, 1798–1805.

Redman, J. A., S. L. Walker, and M. Elimelech (2004), Bacterial adhesion and transport in porous media: Role of the secondary energy minimum, *Environ. Sci. Technol.*, *38*, 1777–1785.

Schijven, J. K., and S. M. Hassanizadeh (2000), Removal of viruses by soil passage: Overview of modeling, processes, and parameters, *Crit. Rev. Environ. Sci. Technol.*, *30*, 49–127.

Simoni, S. F., H. Harms, T. N. P. Bosma, and A. J. B. Zehnder (1998), Population heterogeneity affects transport of bacteria through sand columns at low flow rates, *Environ. Sci. Technol.*, *32*, 2100–2105.

Simunek, J., M. T. van Genuchten, and M. Sejna (2005), The HYDRUS-1D software package for simulating the one-dimensional movement of water, heat, and multiple solutes in variably-saturated media, version 3.0, *HYDRUS Software Ser. 1*, 240 pp., Dep. of Environ. Sci., Univ. of Calif., Riverside.

Tan, Y., J. T. Cannon, P. Baveye, and M. Alexander (1994), Transport of bacteria in an aquifer sand: Experiments and model simulations, *Water Resour. Res.*, *30*, 3243–3252.

Tong, M., X. Li, C. N. Brow, and W. P. Johnson (2005a), Detachment-influenced transport of an adhesion-deficient bacterial strain within water-reactive porous media, *Environ. Sci. Technol.*, *39*, 2500–2508.

Tong, M., T. A. Camesano, and W. P. Johnson (2005b), Spatial variation in deposition rate coefficients of an adhesion-deficient bacterial strain in quartz sand, *Environ. Sci. Technol.*, *39*, 3679–3687.

Tufenkji, N., and M. Elimelech (2005a), Spatial distributions of *Cryptosporidium* oocysts in porous media: Evidence for dual model deposition, *Environ. Sci. Technol.*, *39*, 3620–3629.

Tufenkji, N., and M. Elimelech (2005b), Breakdown of colloid filtration theory: Role of the secondary energy minimum and surface charge heterogeneities, *Langmuir*, *21*, 841–852.

Tufenkji, N., J. A. Redman, and M. Elimelech (2003), Interpreting deposition patterns of microbial particles in laboratory-scale column experiments, *Environ. Sci. Technol.*, *37*, 616–623.

Tufenkji, N., G. F. Miller, J. N. Ryan, R. W. Harvey, and M. Elimelech (2004), Transport of *Cryptosporidium* oocysts in porous media: Role of straining and physicochemical filtration, *Environ. Sci. Technol.*, *38*, 5932–5938.

U.S. Environmental Protection Agency (USEPA) (1997), National water quality inventory, report to Congress, *Rep. EPA 841-R-97-008*, Washington, D. C.

U.S. Environmental Protection Agency (USEPA) (2000), National primary drinking water regulations: Ground water rule, proposed rule, *Fed. Reg.*, *10*, 30,194–30,274.

Zhang, P., W. P. Johnson, T. D. Scheibe, K. Choi, F. C. Dobbs, and B. J. Mailloux (2001), Extended tailing of bacteria following breakthrough at the Narrow Channel Focus Area, Oyster, Virginia, *Water Resour. Res.*, *37*, 2687–2698.

S. A. Bradford, George E. Brown Jr. Salinity Laboratory, ARS, USDA, 450 West Big Springs Road, Riverside, CA 92507-4617, USA. (sbradford @ ussl.ars.usda.gov)

J. Simunek, Department of Environmental Sciences, University of California, Riverside, CA 92521, USA.

S. L. Walker, Department of Chemical and Environmental Engineering, University of California, Riverside, CA 92521, USA.